# Wild animals suppress the spread of socially transmitted misinformation

Ashkaan K. Fahimipour[a,b,1] (ID), Michael A. Gil[c] (ID), Maria Rosa Celis[b] (ID), Gabriel F. Hein[d] (ID), Benjamin T. Martin[e], and Andrew M. Hein[f,1] (ID)

Understanding the mechanisms by which information and misinformation spread through groups of individual actors is essential to the prediction of phenomena ranging from coordinated group behaviors to misinformation epidemics. Transmission of information through groups depends on the rules that individuals use to transform the perceived actions of others into their own behaviors. Because it is often not possible to directly infer decision-making strategies in situ, most studies of behavioral spread assume that individuals make decisions by pooling or averaging the actions or behavioral states of neighbors. However, whether individuals may instead adopt more sophisticated strategies that exploit socially transmitted information, while remaining robust to misinformation, is unknown. Here, we study the relationship between individual decision-making and misinformation spread in groups of wild coral reef fish, where misinformation occurs in the form of false alarms that can spread contagiously through groups. Using automated visual field reconstruction of wild animals, we infer the precise sequences of socially transmitted visual stimuli perceived by individuals during decision-making. Our analysis reveals a feature of decision-making essential for controlling misinformation spread: dynamic adjustments in sensitivity to socially transmitted cues. This form of dynamic gain control can be achieved by a simple and biologically widespread decision-making circuit, and it renders individual behavior robust to natural fluctuations in misinformation exposure.

misinformation | decision-making | social networks | higher-order interactions | behavioral control

For social organisms, the actions of others provide constant sources of sensory stimulation that help guide effective decision-making (1–3). Cues generated by others can encode valuable information about the environment, for example, by providing access to stimuli beyond an individual's own sensory limits (2, 4) or early warning of impending events (4, 5). But, socially transmitted cues also convey misinformation—erroneous, outdated, or easily misinterpreted content that impedes effective decision-making (6–9).

In natural ecosystems, one of the most widespread forms of misinformation occurs as a result of false alarms, wherein an individual animal in a group makes a decision to produce an alarm signal or initiate an escape maneuver in the absence of a true threat (7, 9–12). This initial action produces sensory stimuli that can be perceived by others in the group as an indication of danger (8), resulting in a cascade of erroneous escape responses that can propagate contagiously (13, 14). Basing decisions on this form of misinformation can be costly (9, 15), suggesting that selection may favor decision-making strategies that are robust to misinformation exposure.

In stable, long-term groups, animals may be able to infer the reliability of a signal using knowledge about the sender (1). However, in many situations such as in crowds (16), automobile traffic (17), bird flocks (8, 18), and feeding aggregations (3, 19), decisions must be made rapidly (7, 17) in large or ephemeral collectives (20), where using foreknowledge of the reliability of all senders is impossible. Behavioral and neurophysiological studies suggest that relatively simple behavioral strategies control decision-making in many such settings (16, 17, 19, 21–23). But, it is not known whether these strategies somehow account for the possibility of exposure to misinformation.

## Results

To address this question, we deployed camera observatories in a coral reef to continuously record behavioral decision-making of wild, mixed-species groups of foraging fish (Fig. 1; *Methods* and *SI Appendix*). Like other social animals (5, 8, 13), reef fish exhibit collective escape responses, wherein individuals within a group cease feeding and flee in rapid succession (19, 20). Misinformation is produced in the form of escape responses in the absence of true shared threats (i.e., predators), which can spread through groups as false alarm cascades.

## Significance

Despite the benefits of learning about the world through social ties, social connections also provide a conduit for misinformation. Using underwater camera observatories to record the behavior of foraging coral reef fishes, we find that these animals produce and perceive visual motion cues produced by others, thereby forming dynamic information networks. These networks are surprisingly robust to false alarms that occur when one individual flees in the absence of a true shared threat. By reconstructing visual sensory inputs to each animal, we show that this robustness to misinformation about threats inherits from a specific property of their decision-making strategy: dynamic adjustments in sensitivity to socially acquired information. This property can be achieved through a simple and biologically widespread decision-making circuit.
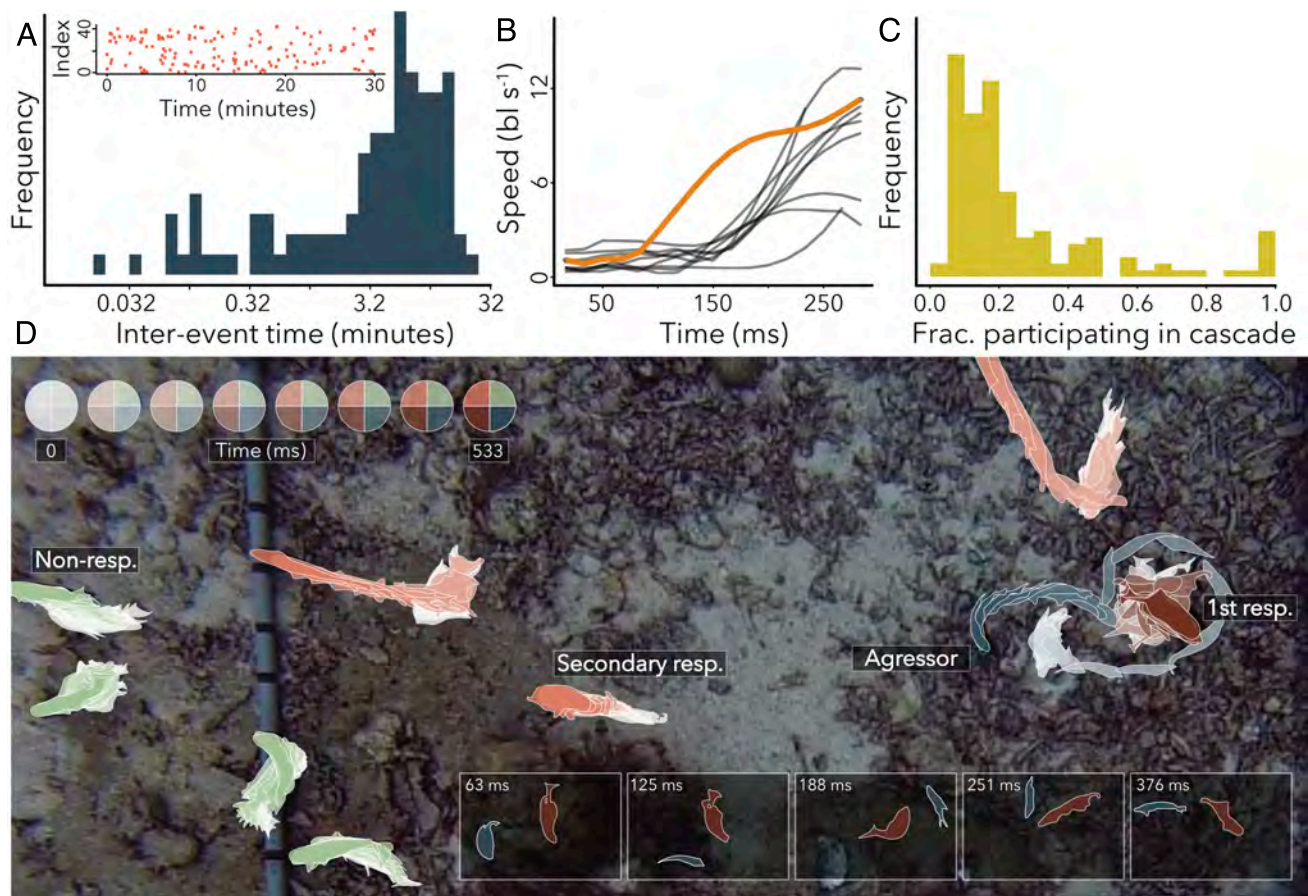
**Fig. 1.** Natural escape cascades. (*A*) 42 empirical time series of escape event initiation times (red raster) from observations of unperturbed groups of wild coral reef fish. The histogram shows the distribution of interevent time intervals. (*B*) Swimming speed profiles for all responding fish in an example escape cascade (first responder in orange). (*C*) Fraction of individuals responding in natural escape events shown in (*A*). (*D*) Example escape event. The aggressor (blue) rapidly approaches another individual (first responder, dark red), which exhibits an escape response. Secondary responses by other individuals (pink) follow. Others present do not exhibit escape responses (green). The inset shows the time sequence of aggressor and first responder positions.

In natural foraging collectives, escape events in the absence of true predator threats occur regularly, at a mean rate of one event per 7.7 min (Fig. 1*A*). During these events, one individual in the group (the first responder) exhibits an escape maneuver (24) involving a deep body bend followed by large acceleration and rapid turning (Fig. 1*B* and *SI Appendix*, Fig. S1). This initial response may be followed by a cascade of subsequent responses by other individuals (Fig. 1*B*). Escape behavior of first responders often coincides with the rapid approach of another fish in the group, indicating an aggressive interaction (Fig. 1*D*, and *SI Appendix*, Fig. S2), to which an escape maneuver is an appropriate reaction. However, aggressive interactions are seldom directed at secondary responders (*SI Appendix*, Fig. S2), suggesting that secondary responses are erroneous reactions to a simple form of misinformation: stimuli produced during the interaction between the aggressor and first responder.

While some escape events involve large response cascades (Fig. 1 *B*–*C*), most involve only the first responder. The rarity of large false alarm cascades suggests that individuals may employ a decision strategy that is responsive to true threats, like an approaching aggressor, while being robust to the misinformation produced during interactions between other individuals in the group.

In fish, escape responses are controlled by specialized neural circuits that process incoming sensory stimuli, including visual motion stimuli (19), and route signals to premotor neurons in the hindbrain (25–27). Experimentally presented visual motion stimuli are sufficient to trigger escape maneuvers of coral reef fish in a manner consistent with known features of these circuits (19). We therefore hypothesized that natural escape events (Fig. 1 *A*–*D*) are initiated and spread through visual stimuli produced when individuals in the group move.

To test this, we reconstructed visual sensory information available to each animal prior to and during escape events (Fig. 2*A*; and *SI Appendix*). As they moved, fish produced strong motion stimuli visible to others (looming motion, i.e., apparent rate of expansion of an approaching object; translation, i.e., apparent rate of lateral motion of the object; *SI Appendix*). These stimuli routinely exceed magnitudes shown in past laboratory experiments to trigger escape behavior (*SI Appendix*, Fig. S3, (24–27)). Escape responses in our data were preceded by periods of strong looming and translation stimuli from neighbors (*SI Appendix*, Fig. S4); and during escapes, responders turned away from the neighbor producing the strongest stimulus (Fig. 2*B*)—a pattern previously shown using experimentally evoked escape responses (28). Importantly, individuals that responded also produced strong motion stimuli visible to others (Fig. 2 *C* and *D*), providing a potential mechanism by which the response of one individual could trigger others to respond, thereby propagating a response cascade. To further test this possibility, we developed a sensory decision-making model that related incoming sensory input to the decision to respond or not to respond.
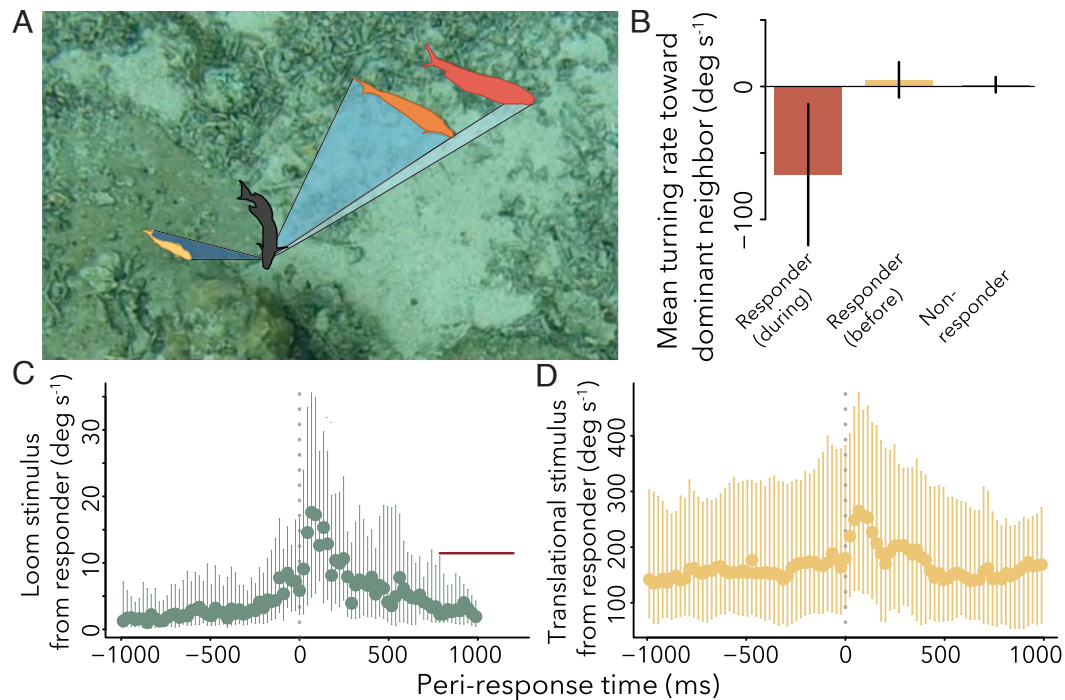
**Fig. 2.** Visual field reconstruction and stimuli during escape events. (*A*) All animals were tracked in videos (single frame shown) using an automated tracking pipeline (*SI Appendix*). A raycasting algorithm (19) and pinhole camera model (22) were used to estimate the projection of each neighbor on the retina of the focal individual (black-outlined individual). (*B*) Mean turning rate toward dominant neighbor (neighbor producing strongest loom) for the responding fish within 200 ms of escape initiation time, "responders (during)"; the same fish during periods prior to the event, "responders (before)"; and fish present during the escape event that did not respond. Negative values indicate turning away from the neighbor. (*C*) Median loom rate and median translation rate (*D*) produced by the first responder as perceived by other individuals present. The red line in (*C*) shows the median of putative loom thresholds reported in previous studies (24). Bars in all panels indicate the 25th and 75th percentiles.

**Prevailing Models Do Not Describe Responses to Visual Misinformation.** Two prevailing hypotheses describe how a decision-maker might operate on sensory information from its neighbors when making behavioral decisions (*SI Appendix,* Table S1). Under the first hypothesis, which we refer to as pooling, individuals sum sensory input over neighbors (29), respond independently to input from each neighbor (30), or base responses on the strongest input produced by a set of neighbors via selective attention (28). Under the second hypothesis, which we refer to as averaging, individuals average sensory input from different neighbors (21) or average the responses to input from multiple neighbors (22). To determine whether one of these strategies is consistent with observed escape decision-making, we compared a diverse set of pooling and averaging strategies (*Methods*; and *SI Appendix,* Table S1). Our analysis revealed that none of these strategies accurately predicted which individuals would respond during escape events and which would not (Fig. 3*A*, models p1-p8 and a1-a2). These strategies were particularly bad at describing the behavior of secondary responders and nonresponders (Fig. 3*A*, *Middle*).

**Decision-Making is Robust to Large Changes in Visual Sensory Input.** To understand why previously proposed models of decision-making poorly described escape decisions of reef fish, we analyzed empirical patterns of sensory input perceived by fish during escape events. In reef fish foraging aggregations, the local density of individuals continually fluctuates as individuals enter and leave foraging areas (20). A curious feature of escape events in our data (Fig. 1 *A* and *C*) is that although the total and maximum strengths of visual motion stimuli vary by more than 10-fold as local density changes (Fig. 3 *B* and *C*), escape cascades are typically small (median size = 1 responder; Fig. 1*C*) and cascade size is uncorrelated with the density of the group

during the event (Spearman rank correlation between cascade size and density: $\rho = 0.093$; linear regression, $P = 0.26$ and $R^2 = 8.6 \times 10^{-3}$). This suggests that the strategy individuals use to control escape decision-making may involve somehow adjusting sensitivity, or gain, applied to sensory input as the overall level of input changes.

**A Model of Decision-Making with Dynamic Gain Control.** Dynamic rescaling of sensitivity is common within sensory organs such as the vertebrate retina (35) that operate across a wide dynamic range of inputs. We asked whether individuals might use a behavioral analog of this process, response rescaling (36), to dynamically adjust behavioral responsivity as the intensity and frequency of stimuli from neighbors change.

One mechanism by which a decision-maker can achieve dynamic changes in sensitivity to incoming stimuli involves the accumulation of past sensory evidence over time (37–39). By remembering recently experienced sensory stimulus values, sensitivity to new incoming stimuli can be tuned up or down based on the stimuli an individual has experienced in the recent past (40). In *Methods*, we derive a simple decision rule with this property (Fig. 3*D*), which can be written as $D(t) = D^\star + \mathbf{M}(t)\mathbf{w}\left[\gamma + m(t)\right]^{-1}$, where $\mathbf{M}(t) = \{\sum_i S_i'(t), \sum_i T_i(t)\}$ is the vector of perceived looming and translational motion summed over all neighbors, $\mathbf{w}$ is a vector of constant weights applied to these motion stimuli, $D^\star$ and $\gamma$ are constants, and $m(t) = \omega \int_{-\infty}^{t} e^{-\frac{t-s}{\tau}} \mathbf{M}(s)\mathbf{w}\,ds$ is an exponentially weighted integral of the past history of sensory input from neighbors with constant, $\omega$, and decay timescale, $\tau$. The probability to respond to visual stimuli in a small time increment is given by $p(t) = (1 + e^{-D(t)})^{-1}$. In this model, increasing sensory input increases the probability to respond but simultaneously lowers
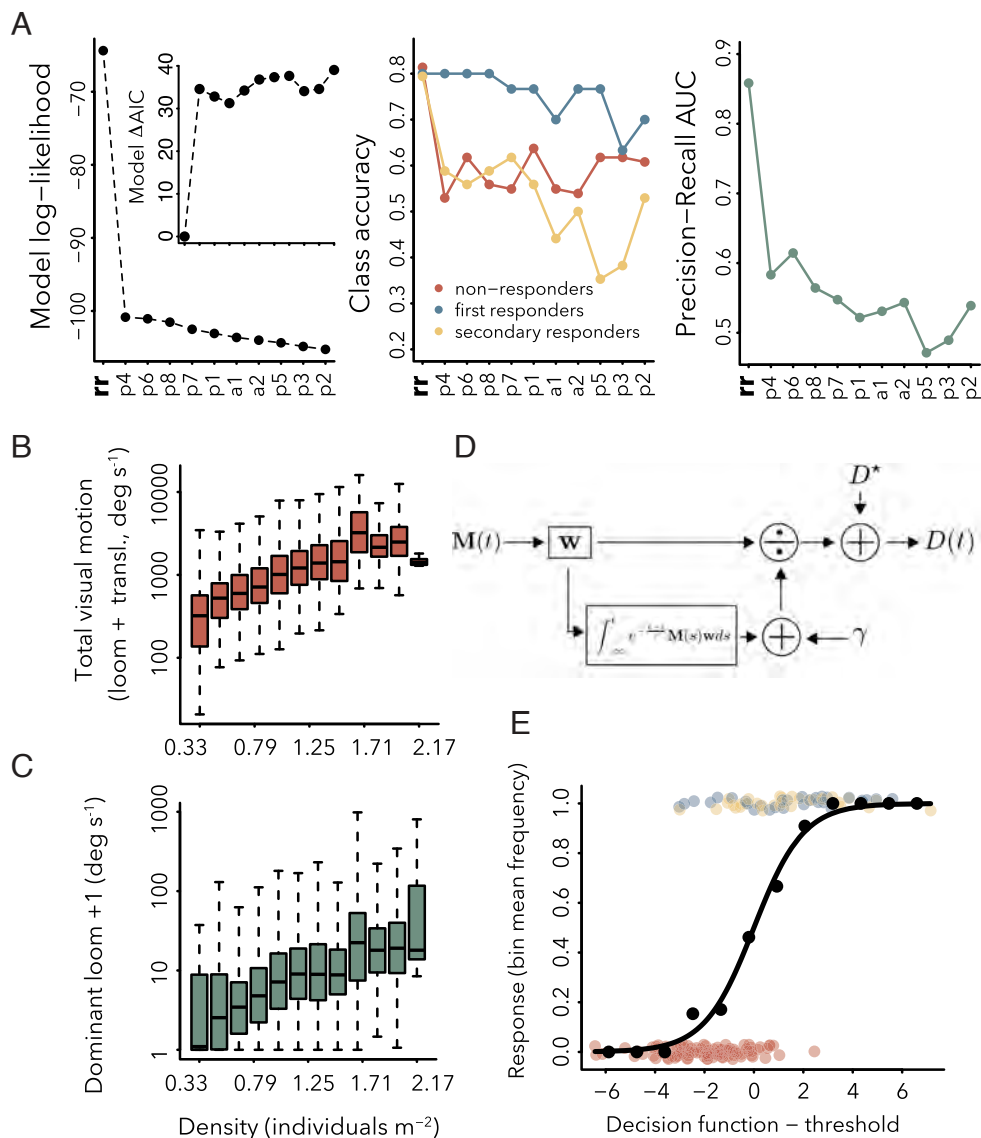
**Fig. 3.** Decision-making models and density scaling of sensory input. (*A*) Performance of averaging ("a"), pooling ("p"), and response-rescaling ("**rr**") models: model log-likelihood (*Left*, inset shows ΔAIC with models ordered as in *A Left*), prediction accuracy for different response classes (center), and precision-recall area under the curve (PR AUC, right; *SI Appendix*, Tables S1–S2 for full model descriptions). ΔAIC defined as the difference between the Akaike information criterion value (31), of each model and that of the model with the lowest AIC in the model set (**rr**). (*B*) Density-scaling of total visual motion input from neighbors and (*C*) looming from the neighbor producing the strongest loom signal. (*D*) Diagram of response-rescaling model structure (*Text*, *Methods* for description of symbols and model derivation). (*E*) Observed responses colored points, colors as in (*A*) center; points vertically jittered, empirical fraction responding (black points), and predicted (black line) response probability from the response-rescaling model. Note on (*A*): We were unable to fit standard phenomenological formulations of simple (32, 33) and fractional contagion (32, 34) models to this dataset because, under both models, the probability to respond when no neighbor has yet responded is zero; thus, these models cannot predict the onset of escape events. Nevertheless, we analyze predicted spreading properties of these models after cascade onset in Fig. 4.

the gain applied to future input, creating an opponency between excitatory and inhibitory effects of visual motion stimuli. In *Methods*, we show that the dynamic gain control inherent in this model can be achieved by a neural circuit containing just three interlinked populations of neurons. Unlike previously proposed pooling and averaging strategies (Fig. 3*A*), this response-rescaling strategy accurately predicts the behavior of first, secondary, and nonresponders (Fig. 3*A*, model *rr*; Fig. 3*E*).

**Individual Decision-Making Strategies Determine Patterns of Misinformation Spread through Populations.** To understand how this decision-making strategy may impact the spread of misinformation, we developed a spatially explicit, empirically calibrated computational model that simulates populations of

individual agents, each of which perceives visual stimuli from others and makes decisions to flee or not to flee based on these stimuli (*Methods*; *SI Appendix*). In each simulation, we modeled an aggressive interaction between a random pair of nearest neighbors in the population (Fig. 4) and ask how misinformation generated through the interaction travels through the network defined by exchanges of visual information among neighbors.

In the past, many studies of behavioral contagion in social groups have assumed one of two models for behavioral spread among agents: simple contagion (13, 21, 30, 33), under which an individual's probability to respond is independently influenced by each of its responding neighbors, and fractional contagion (13, 14, 21, 32, 34), under which an individual's probability to respond depends on the fraction of its neighbors currently
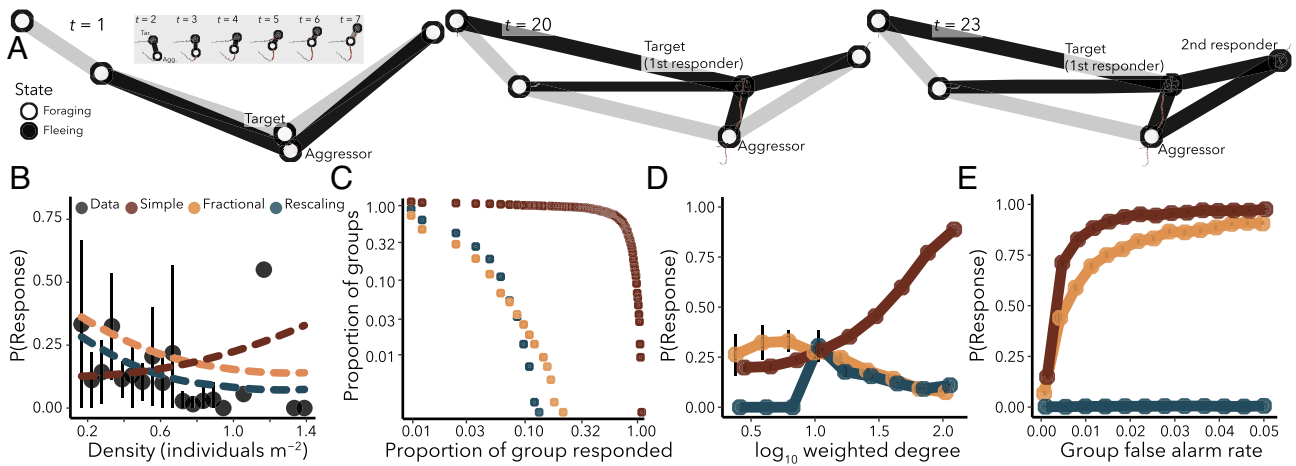
**Fig. 4.** Misinformation spread in populations of decision-makers (computational model). (*A*) Time sequence of simulated interaction between aggressor and first responder along with subsequent response of a secondary responder. Edges are drawn between individuals that are within the visual range of one another. (*B*) Empirical per-capita response probability (points and error bars) as a function of density and relationships predicted by response-rescaling (blue), simple (red), and fractional contagion (yellow) models (*SI Appendix*) (*C*) One minus the cumulative distribution function of cascade sizes produced by response rescaling, simple contagion, and fractional contagion. (*D*) Response probability conditional on exposure to a misinformation cascade as a function of an individual's weighted degree in the social network. Note the relatively high response probability of low-degree nodes for simple and fractional contagion versus low response probability for response rescaling (*E*) Probability to respond to misinformation as a function of the per capita false alarm rate (i.e., probability of each agent to initiate a false alarm in each timestep; *SI Appendix*) of other individuals in the population.

responding (*SI Appendix*). To understand whether either of these phenomenological models accurately approximates the dynamics of behavioral spread generated under the response-rescaling strategy inferred from our data, we compared patterns of misinformation spread in simulated populations of individuals that use response rescaling to patterns observed in simulated populations that use simple or fractional contagion.

The response rescaling population exhibited a decreasing per capita response probability with increasing density consistent with data (Fig. 4*B*). This led to mean cascade sizes that were invariant to density (*SI Appendix*, Fig. S6*A*). Simulations assuming behavioral spread via simple contagion could not reproduce this pattern, whereas those that assumed fractional contagion produced predictions similar to those of response scaling. The population following fractional contagion also exhibited a similar distribution of cascade sizes to the response-rescaling population (Fig. 4*C*).

Fractional contagion shares several spreading properties with response rescaling, in part, because it captures a qualitative property of decision-making in our data: On average, as an individual acquires more neighbors, they require more sensory input in order to respond (*SI Appendix*, Fig. S5). Thus, rather than acting as superspreaders (Fig. 4*D*, red curve), highly connected individuals are relatively unlikely to respond to misinformation when they are exposed to it (Fig. 4*D*, blue and orange curves). This property makes individual decision-making robust to changes in misinformation exposure that occur as density and, as a consequence, local connectivity increases (*SI Appendix*, Fig. S6*B*). However, the fractional contagion model overestimates response probabilities for individuals with very few neighbors (Fig. 4*D*).

Density fluctuations are one source of variation in natural groups (20) that impacts exposure to misinformation. Another source is caused by continuous fluctuations in the phenotypic (i.e., species) composition of groups as individuals enter and exit foraging areas. These fluctuations in phenotypic composition lead to variation in the rate at which misinformation is produced due to behavioral differences among species (*SI Appendix*, Fig. S7); some species frequently trigger escape events by fleeing in

the absence of predators, whereas others do so infrequently. To understand how individual decision-making is influenced by changes in the rate at which misinformation is produced, we performed simulations in which a focal individual in the population made decisions to escape using either response rescaling, simple contagion, or fractional contagion; we then varied the rate at which other individuals in the population generate misinformation by spontaneously fleeing (*SI Appendix* and Fig. 4*E*).

The probability that an individual using simple or fractional contagion will respond to misinformation increases rapidly to near one as the origination rate of misinformation increases. In contrast, individuals that use response rescaling maintain a low probability of responding to misinformation that is nearly invariant to the rate at which misinformation is produced (Fig. 4*E*, blue line). This difference in robustness of decision-making inherits from the dynamic nature of gain control under response rescaling (*SI Appendix*): As individuals perceive more frequent bursts of strong sensory input from neighbors, inhibition lowers the gain applied to future visual stimuli from those neighbors, thereby lowering responsivity. In this sense, escape responses are driven not simply by motion, but by motion that is surprising. Simple and fractional contagion lacks this property of temporal adaptation, and decision-making in those models is fragile under changes in the rate of production of misinformation.

## Discussion

Using socially transmitted information while at the same time avoiding basing decisions on misinformation poses a fundamental conflict for the animal brain. Our results suggest that animals may at least partially resolve this conflict by dynamically adjusting their sensitivity to stimuli through simultaneous excitation and inhibition within decision-making circuits. From the perspective of an individual making decisions across changing sensory conditions, this decision-making strategy allows the individual to adjust sensitivity to socially transmitted information as the overall magnitude and frequency of stimuli change. At the scale of groups and populations, this form of social decision-making

suppresses large-scale misinformation cascades, resulting instead in shorter sequences of behavioral responses that are localized in space and brief in duration.

Many species learn about events in the world around them using sensory systems that exhibit temporal adaptation to incoming stimuli (35, 36, 40–43). This adaptation can effectively rescale measurements or internal representations of sensory cues based on the recent history of past inputs, conferring a mechanism for dynamic control of behavioral responses (36, 43, 44). Moreover, recent models of opinion formation in social networks have suggested that temporal integration and rescaling (45) are crucial for accurately representing processes such as polarization in human systems (46). Our results add to this picture, by demonstrating that dynamic gain control can determine the susceptibility of individuals to socially transmitted misinformation and the degree to which misinformation spreads through populations. It will be interesting to investigate whether the mechanisms revealed here are also important in driving individual decision-making and misinformation spread in other biological and social systems.

## Materials and Methods

**Data Collection.** Data were collected in lagoon reefs of Mo'orea French Polynesia. Polyvinyl carbonate (PVC) camera frames (2-m width × 6-m length × 2-m depth) were deployed in lagoon sites on the north shore of the island. Deployment locations were typical of lagoon habitat and were characterized by a shallow (2.5-m depth) reef flat, comprising primarily pavement and coral rubble adjacent to live and dead colonies of massive and submassive *Porites* corals of 0.5- to 2-m height. Reef fish use these types of open reef flats between coral structures as foraging areas (20). In each foraging area, a camera frame was mounted using concrete substrate mounts. Foraging areas were filmed continuously from above using downward-facing cameras shooting at either 30 or 60 frames per second (GoPro Hero 3 or Hero 4). Footage used in analyses was collected under unperturbed conditions (i.e., no experimental perturbations were applied), a minimum of 30 min after cameras were deployed and researchers had vacated the area. Details on automated animal tracking and visual field reconstruction are described in *SI Appendix*.

**Comparing Models of Individual Decision-Making.** The set of plausible models describing how an individual decision-maker might integrate and operate on sensory data from multiple neighbors is vast. We therefore focused on a set of models based on features of decision-making previously described in the perceptual decision-making literature on the basis of behavioral or neurophysiological evidence (*SI Appendix*, Table S1). Multisource perceptual decision-making models can be organized broadly into two classes on the basis of their assumptions about how stimuli from neighbors are integrated during decision-making: pooling models (28–30), and averaging models (13–15, 21, 47). We consider variants of common decision-making models for each candidate class, including models in which raw visual stimuli are linearly combined to form visual features (29, 30) as well as models in which driving sensory features are nonlinear combinations of raw inputs (19, 48). Details on models and model-fitting are provided in *SI Appendix*, *Defining the Model Set* and *Estimating Model Parameters*.

**Derivation of Response-Rescaling Model.** We tested a suite of previously proposed decision-making models and found that none accurately predicted individuals' responses to incoming visual stimuli (Fig. 3). Based on this result and physiological evidence from other systems (35, 36), we hypothesized that individuals may control escape decisions using a rule that dynamically adjusts the gain applied to incoming sensory input based on the recent history of visual input, thereby rescaling their responsivity. This type of dynamic gain control is a hallmark of many sensory systems including the vertebrate visual (35) and auditory systems (40) and the chemosensory and internal signaling systems of bacteria and other cells (36, 41, 43, 44), all of which operate over a wide dynamic range of input magnitudes.

Our work considers a distinct but related problem: controlling responsivity to socially transmitted stimuli amid continual changes in the overall magnitude and frequency of those stimuli. We postulated that robust escape decision-making requires two properties: i) The strength of stimulus necessary to trigger an escape response must vary as the overall magnitude of sensory input changes to allow individuals to maintain sensitivity to changes in visual stimuli when overall visual motion is low and to avoid becoming overly responsive when the overall level of visual motion stimuli increases (*SI Appendix*, Fig. S5), and ii) the sensitivity of the system should vary as the temporal frequency of events that produce strong sensory stimuli but are not indicative of true threats (i.e., visual misinformation) changes. This latter property requires that individuals maintain some memory of stimuli perceived in the recent past and adjust their sensitivity to future stimuli accordingly.

A biologically widespread circuit motif that enables these properties involves fast-timescale excitation by incoming sensory input along with simultaneous inhibition by the same input on a slower timescale (36, 40, 41, 43, 44). We hypothesize that escape decision-making by coral reef fish is driven by a neural circuit with these properties. In particular, we postulate that looming, $S'(t)$, and translational stimuli, $T(t)$, are summed over a focal individual's visual field, such that the driving input for downstream computations is summed visual motion input, $\mathbf{M}(t) = \{\sum_i S'_i(t), \sum_i T_i(t)\}$. Pooled looming and translation stimuli are then scaled and summed to yield an internal variable, $u(t) = \mathbf{M}(t)\mathbf{w}$, where $\mathbf{w} = \{w_{S'}, w_T\}$ is a vector of constant weights.

The quantity $u(t)$ could be encoded, for example, in the firing rate of a population of neurons that provides the input to the rescaling circuit. The rescaling circuit involves the firing rate of the input population $u$, the firing rate of a memory (40) population, $m$, and firing rate of a readout population, $y$, with leakage rate $1/\rho$. The memory population is excited by $u$ and returns to its baseline activity with rate $1/\tau$ in the absence of input from $u$. We take the dynamics of $m$ and $y$ to be given by:

$$dm/dt = \omega u - \frac{1}{\tau}m \qquad dy/dt = \alpha\frac{u}{m} - \frac{1}{\rho}y, \qquad [1]$$

where $\omega$ and $\alpha$ are constants. Assuming that the dynamics of $y$ are fast relative to those of $m$, we obtain an expression for the firing rate of the readout population,

$$y(t) = \alpha\rho\frac{u}{m}, \qquad [2]$$

which is proportional to the input, rescaled by the activity of the memory population, $m$.

The system specified by Eq. **1** can be viewed as a deterministic system of leaky evidence accumulators (49, 50). Fitting such systems directly to behavioral data can result in model parameters being unidentifiable (50, 51). However, because we are primarily interested in the timescale over which behavioral decisions are made, which is significantly longer than the fastest timescale of neural dynamics, we exploit this separation of timescales to simplify the model. In particular, assuming $t \gg 0$ yields an expression for the memory population's activity:

$$m(t) = \omega \int_{-\infty}^{t} e^{-\frac{t-s}{\tau}} u(s)ds. \qquad [3]$$

In practice, for very low activity of the memory population (i.e., $m \rightarrow 0$), the output of Eq. **2** can become extremely sensitive to fluctuations in input. We therefore introduce a constant, $\gamma$. (Note that an alternative model could apply a filter or gating term to control sensitivity at very low input values.) This gives $y(t) = \alpha\rho\frac{u}{\gamma+m}$. Taking the "sensory feature" that drives decision-making to be defined by $F(t) = y(t)/(\alpha\rho)$ gives

$$F(t) = \frac{\mathbf{M}(t)\mathbf{w}}{\gamma + m(t)}. \qquad [4]$$

This quantity is assumed to drive decision-making through the function $D(t) = D^{\star} + F(t)$.

One candidate module within the fish visual escape circuit (52) that may be capable of performing the computations implied by Eq. **1** involves populations

of glycinergic (53) and dopaminergic (54) interneurons and tectal projection neurons in the fish hindbrain that receive input from the optic tectum. Although the precise computational properties and connectivity of these populations are still unclear, they have been implicated in a feedforward inhibitory circuit believed to gate escape responses to different types of visual stimuli (54). For this reason, we formulated Eq. **1** as a feed-forward inhibitory circuit. However, we also note that other circuit motifs including circuits with integral feedback and logarithmic feedback (43, 44) are capable of producing rescaling properties similar to those of Eq. **4**.

**Agent-Based Model.** We studied the spread of misinformation in simulated networks of agents who move and sense each other on a featureless 2-dimensional plane. In these social networks, agents can be either in the *foraging* or the *fleeing* state based on their current and past perceived motion of neighbors. Model parameters, including those that control agent movement, sensing, and decision-making, were set to their corresponding empirical estimates (*SI Appendix*, Table S3). Full details on the individual-based model formulation can be found in *SI Appendix*, and an implementation for the Julia 1.7.1 programming language is provided at https://github.com/AshkaanF/scaredyfish.

Two primary simulation-based experiments were performed to understand and compare the dynamics of populations comprising individuals following the response-rescaling rule (Eq. **4**), to phenomenological approximations of social contagion defined by widely studied simple and fractional contagion rules (13–15, 21, 30, 32–34) (*SI Appendix* for model formulations). In the first set of simulations, we sought to understand how group density, agent connectivity, and decision-making rules interact to influence the likelihood of responding to a unit of misinformation, which originated from a simulated aggressive encounter between a randomly chosen pair of nearest neighbors in the population (*SI Appendix, Numerical Experiments for Misinformation Spread*).

In these simulations, misinformation spreads through the group as agents respond to the initial burst of motion from the aggression event as well as subsequent responses.

To understand how variation in the frequency of misinformation origination events would impact decision-making in individuals, we performed a second set of computational simulations holding density at its empirical average, $\hat{N} \sim 0.8$ individuals m$^{-2}$. Here, a focal individual is granted decision-making capabilities (i.e., the response-rescaling, simple, or fractional contagion rules) and embedded in a population of spontaneously startling individuals who switch to the *flee* state with a constant probability $p$ in each time step. Additional details on model formulation and simulations are provided in *SI Appendix*.

Author affiliations: [a]Department of Biological Sciences, Florida Atlantic University, Boca Raton, FL 33431; [b]Institute of Marine Sciences, University of California Santa Cruz, Santa Cruz, CA 95060; [c]Department of Ecology & Evolutionary Biology, University of Colorado Boulder, Boulder, CO 80309; [d]OpenSpace Inc., San Francisco, CA 94108; [e]Institute for Biodiversity & Ecosystem Dynamics, University of Amsterdam, 1090 GE Amsterdam, The Netherlands; and [f]Department of Computational Biology, Cornell University, Ithaca, NY 14850

1. C. Canteloup, W. Hoppitt, E. van de Waal, Wild primates copy higher-ranked individuals in a social transmission experiment. *Nat. Commun.* **11**, 1–10 (2020).
2. A. Flack, M. Nagy, W. Fiedler, I. D. Couzin, M. Wikelski, From local collective behavior to global migratory patterns in white storks. *Science* **360**, 911–914 (2018).
3. S. R. Dall, L. A. Giraldeau, O. Olsson, J. M. McNamara, D. W. Stephens, Information and its use by animals in evolutionary ecology. *Trends Ecol. Evol.* **20**, 187–193 (2005).
4. N. V. Carlson, E. Greene, C. N. Templeton, Nuthatches vary their alarm calls based upon the source of the eavesdropped signals. *Nat. Commun.* **11**, 1–7 (2020).
5. K. Meise, D. W. Franks, J. Bro-Jørgensen, Alarm communication networks as a driver of community structure in African savannah herbivores. *Ecol. Lett.* **23**, 293–304 (2020).
6. K. N. Laland, K. Williams, Social transmission of maladaptive information in the guppy. *Behav. Ecol.* **9**, 493–499 (1998).
7. L. A. Giraldeau, T. J. Valone, J. J. Templeton, Potential disadvantages of using socially acquired information. *Phil. Trans. Roy. Soc. Lond. B* **357**, 1559–1566 (2002).
8. S. L. Lima, Collective detection of predatory attack by social foragers: Fraught with ambiguity? *Anim. Behav.* **50**, 1097–1108 (1995).
9. G. Beauchamp, Determinants of false alarms in staging flocks of semipalmated sandpipers. *Behav. Ecol.* **21**, 584–587 (2010).
10. B. C. Wheeler, K. Hammerschmidt, Proximate factors underpinning receiver responses to deceptive false alarm calls in wild tufted capuchin monkeys: Is it counterdeception? *Am. J. Primatol.* **75**, 715–725 (2013).
11. B. C. Wheeler, Monkeys crying wolf? Tufted capuchin monkeys use anti-predator calls to usurp resources from conspecifics. *Proc. R. Soc. B: Biol. Sci.* **276**, 3013–3018 (2009).
12. T. Flower, Fork-tailed drongos use deceptive mimicked alarm calls to steal food. *Proc. R. Soc. B: Biol. Sci.* **278**, 1548–1555 (2011).
13. S. B. Rosenthal, C. R. Twomey, A. T. Hartnett, H. S. Wu, I. D. Couzin, Revealing the hidden networks of interaction in mobile animal groups allows prediction of complex behavioral contagion. *Proc. Natl. Acad. Sci. U.S.A.* **112**, 4690–4695 (2015).
14. M. M. Sosna *et al.*, Individual and collective encoding of risk in animal groups. *Proc. Natl. Acad. Sci. U.S.A.* **116**, 20556–20561 (2019).
15. W. Poel, et al., Subcritical escape waves in schooling fish. *Sci. Adv.* **8**, eabm6385 (2022).
16. M. Moussaïd, D. Helbing, G. Theraulaz, How simple rules determine pedestrian behavior and crowd disasters. *Proc. Natl. Acad. Sci. U.S.A.* **108**, 6884–6888 (2011).
17. G. Markkula, Z. Uludağ, R. M. Wilkie, J. Billington, Accumulation of continuously time-varying sensory evidence constrains neural and behavioral responses in human collision threat detection. *PLoS Comput. Biol.* **17**, e1009096 (2021).
18. M. Ballerini *et al.*, Interaction ruling animal collective behavior depends on topological rather than metric distance: Evidence from a field study. *Proc. Natl. Acad. Sci. U.S.A.* **105**, 1232–1237 (2008).
19. A. M. Hein, M. A. Gil, C. R. Twomey, I. D. Couzin, S. A. Levin, Conserved behavioral circuits govern high-speed decision-making in wild fish shoals. *Proc. Natl. Acad. Sci. U.S.A.* **115**, 12224–12228 (2018).
20. M. A. Gil, A. M. Hein, Social interactions among grazing reef fish drive material flux in a coral reef ecosystem. *Proc. Natl. Acad. Sci. U.S.A.* **114**, 4703–4708 (2017).
21. W. Poel, C. Winklmayr, P. Romanczuk, Spatial structure and information transfer in visual networks. *Front. Phys.* 623 (2021).

22. R. Harpaz, M. N. Nguyen, A. Bahl, F. Engert, Precise visuomotor transformations underlying collective behavior in larval zebrafish. *Nat. Commun.* **12**, 1–14 (2021).
23. J. M. Kappel, et al., Visual recognition of social signals by a tecto-thalamic neural circuit. *Nature* 1–7 (2022).
24. P. Domenici, The visually mediated escape response in fish: Predicting prey responsiveness and the locomotor behaviour of predators and prey. *Mar. Freshw. Behav. Physiol.* **35**, 87–110 (2002).
25. I. Temizer, J. C. Donovan, H. Baier, J. L. Semmelhack, A visual pathway for looming-evoked escape in larval zebrafish. *Curr. Biol.* **25**, 1823–1834 (2015).
26. T. W. Dunn *et al.*, Neural circuits underlying visually evoked escapes in larval zebrafish. *Neuron* **89**, 613–628 (2016).
27. K. Bhattacharyya, D. L. McLean, M. A. MacIver, Visual threat assessment and reticu-lospinal encoding of calibrated responses in larval zebrafish. *Curr. Biol.* **27**, 2751–2762 (2017).
28. A. M. Fernandes *et al.*, Neural circuitry for stimulus selection in the zebrafish visual system. *Neuron* **109**, 805–822 (2021).
29. C. H. Ferreira, M. A. Moita, Behavioral and neuronal underpinnings of safety in numbers in fruit flies. *Nat. Commun.* **11**, 1–10 (2020).
30. P. Ramdya *et al.*, Mechanosensory interactions drive collective behaviour in *drosophila*. *Nature* **519**, 233–236 (2015).
31. H. Akaike, "Information theory and an extension of the maximum likelihood principle" in *Proceedings of 2nd International Symposium on Information Theory* (Akademiai Kiado, 1973), pp. 267–281.
32. D. J. Watts, A simple model of global cascades on random networks. *Proc. Natl. Acad. Sci. U.S.A.* **99**, 5766–5771 (2002).
33. J. B. Bak-Coleman, et al., Combining interventions to reduce the spread of viral misinformation. *Nat. Hum. Behav.* 1–9 (2022).
34. D. Centola, The spread of behavior in an online social network experiment. *Science* **329**, 1194–1197 (2010).
35. S. M. Smirnakis, M. J. Berry, D. K. Warland, W. Bialek, M. Meister, Adaptation of retinal processing to image contrast and spatial scale. *Nature* **386**, 69–73 (1997).
36. M. D. Lazova, T. Ahmed, D. Bellomo, R. Stocker, T. S. Shimizu, Response rescaling in bacterial chemotaxis. *Proc. Natl. Acad. Sci. U.S.A.* **108**, 13870–13875 (2011).
37. M. Usher, J. L. McClelland, The time course of perceptual choice: The leaky, competing accumulator model. *Psychol. Rev.* **108**, 550 (2001).
38. K. Tsetsos, J. Gao, J. L. McClelland, M. Usher, Using time-varying evidence to test models of decision dynamics: Bounded diffusion vs. the leaky competing accumulator model. *Front. Neurosci.* **6**, 79 (2012).
39. M. E. Mazurek, J. D. Roitman, J. Ditterich, M. N. Shadlen, A role for neural integrators in perceptual decision making. *Cereb. Cortex* **13**, 1257–1269 (2003).
40. P. Miller, X. J. Wang, Inhibitory control by an integral feedback signal in prefrontal cortex: A model of discrimination between sequential stimuli. *Proc. Natl. Acad. Sci. U.S.A.* **103**, 201–206 (2006).
41. T. M. Yi, Y. Huang, M. I. Simon, J. Doyle, Robust perfect adaptation in bacterial chemotaxis through integral feedback control. *Proc. Natl. Acad. Sci. U.S.A.* **97**, 4649–4653 (2000).

42. G. De Palo *et al*., Common dynamical features of sensory adaptation in photoreceptors and olfactory sensory neurons. *Sci. Rep.* **3**, 1–8 (2013).

43. M. Adler, U. Alon, Fold-change detection in biological systems. *Curr. Opin. Syst. Biol.* **8**, 81–89 (2018).

44. O. Shoval *et al*., Fold-change detection and scalar symmetry of sensory input fields. *Proc. Natl. Acad. Sci. U.S.A.* **107**, 15995–16000 (2010).

45. A. Bizyaeva, A. Franci, N. E. Leonard, Nonlinear opinion dynamics with tunable sensitivity. *IEEE Trans. Autom. Control* (2022).

46. N. E. Leonard, K. Lipsitz, A. Bizyaeva, A. Franci, Y. Lelkes, The nonlinear feedback dynamics of asymmetric political polarization. *Proc. Natl. Acad. Sci. U.S.A.* **118**, e2102149118 (2021).

47. A. Strandburg-Peshkin *et al*., Visual sensory networks and effective information transfer in animal groups. *Curr. Biol.* **23**, R709–R711 (2013).

48. N. Hatsopoulos, F. Gabbiani, G. Laurent, Elementary computation of object approach by a wide-field visual neuron. *Science* **270**, 1000–1003 (1995).

49. R. Bogacz, E. Brown, J. Moehlis, P. Holmes, J. D. Cohen, The physics of optimal decision making: A formal analysis of models of performance in two-alternative forced-choice tasks. *Psychol. Rev.* **113**, 700 (2006).

50. S. Miletić, B. M. Turner, B. U. Forstmann, L. van Maanen, Parameter recovery for the leaky competing accumulator model. *J. Math. Psychol.* **76**, 25–50 (2017).

51. D. Matzke, G. D. Logan, A. Heathcote, A cautionary note on evidence-accumulation models of response inhibition in the stop-signal paradigm. *Comput. Brain Behav.* **3**, 269–288 (2020).

52. E. Marquez-Legorreta, M. Piber, E. K. Scott, "Visual escape in larval zebrafish: Stimuli, circuits, and behavior" in *Behavioral and Neural Genetics of Zebrafish* (Elsevier, 2020), pp. 49–71.

53. M. Koyama, A. Kinkhabwala, C. Satou, S. Higashijima, J. Fetcho, Mapping a sensory-motor network onto a structural and functional ground plan in the hindbrain. *Proc. Natl. Acad. Sci. U.S.A.* **108**, 1170–1175 (2011).

54. Y. Yao *et al*., Visual cue-discriminative dopaminergic control of visuomotor transformation and behavior selection. *Neuron* **89**, 598–612 (2016).